




Article

N-Annulation of the BTI Rylene Imide Organic Building Block: Impact on the Optoelectronic Properties of π -Extended Molecular Structures

José María Andrés Castán ¹, Sana Abidi ^{1,2}, Tatiana Ghanem ¹, Saad Touihri ², Philippe Blanchard ¹ , Gregory C. Welch ³ , Yulian Zagranyski ⁴, Julien Boixel ⁵, Bright Walker ^{6,*}, Pierre Josse ^{1,7,*} , and Clément Cabanetos ^{7,*}

¹ Univ Angers, CNRS, MOLTECH-ANJOU, SFR MATRIX, F-49000 Angers, France

² École Nationale Supérieure d'Ingénieurs de Tunis (ENSIT), 13 Ave Taha Hussein, Tunis 1008, Tunisia

³ Department of Chemistry, University of Calgary, 731 Campus Place N.W., Calgary, AB T2N 1N4, Canada

⁴ Faculty of Chemistry and Pharmacy, University of Sofia, 1 James Bourchier blvd., 1164 Sofia, Bulgaria

⁵ Univ Rennes, CNRS UMR6226, F-35000 Rennes, France

⁶ Department of Chemistry, Kyung Hee University, Seoul 730-701, Republic of Korea

⁷ IRL CNRS 2002, 2BFUEL, CNRS, Yonsei University, Seoul 03722, Republic of Korea

* Correspondence: walker@khu.ac.kr (B.W.); pierre.josse@univ-angers.fr (P.J.); clement.cabanetos@cnrs.fr (C.C.)

Abstract: Benzothioxanthene imide (BTI) has recently emerged as an interesting and promising block for organic electronics. In this contribution, we report on the impact of the N-annulation of the latter dye on the optoelectronic of π -extended molecular structures. To do so, the thiophene-diketopyrrolopyrrole was selected, as central π -conjugated core, and either end-capped with two BTIs or its N-annulated version, namely the TCI. While almost similar band gaps were measured for individual rylene imide dyes, significant differences were highlighted, and rationalized, on their π -extended counterparts.

Keywords: benzothioxanthene imide; thiochromenocarbazole imide; organic synthesis; Structure–property relationships; organic photovoltaics



Citation: Andrés Castán, J.M.; Abidi, S.; Ghanem, T.; Touihri, S.; Blanchard, P.; Welch, G.C.; Zagranyski, Y.; Boixel, J.; Walker, B.; Josse, P.; et al. N-Annulation of the BTI Rylene Imide Organic Building Block: Impact on the Optoelectronic Properties of π -Extended Molecular Structures. *Colorants* **2023**, *2*, 22–30. <https://doi.org/10.3390/colorants2010002>

Academic Editors: Nadia Barbero, Carlotta Pontremoli and Simone Galliano

Received: 1 December 2022

Revised: 22 December 2022

Accepted: 28 December 2022

Published: 30 December 2022



Copyright: © 2022 by the authors. Licensee MDPI, Basel, Switzerland. This article is an open access article distributed under the terms and conditions of the Creative Commons Attribution (CC BY) license (<https://creativecommons.org/licenses/by/4.0/>).

1. Introduction

Over the last decades, rylene-imide-based dyes have attracted considerable research attention [1–3]. Among them, the naphthalene [4–7] and perylene [8–11], functionalized by either one or two imide groups, have quickly emerged as key players in the landscape of organic semiconducting materials. Thanks to the creativity of chemists, a myriad of site-selective functionalizations have been reported, leading to the preparation and characterization of a significant number of new and original π -extended molecular and macromolecular systems [12]. Characterized by remarkable optoelectronic properties, high chemical/thermal stability, and a certain ease of synthesis, a good number of these structures have been successfully used in several devices including organic light emitting diodes (OLEDs), organic field-effect transistors (OFETs) and organic solar cells (OSCs) [1,13–18].

On the fringe of this success story, we have recently focused our attention on another member of this rylene family, namely the benzothioxanthene imide (BTI, Figure 1A). Ignored or simply unknown by the organic electronic community, this sulfur-containing structure was first reported in the early 70 s [19,20] and was mainly used as a fiber dyeing agent and fluorescent probe for bio-imaging [21–23]. In these early reports, it was functionalized solely for grafting and/or solubility reasons on the imide nitrogen atom, however, we have demonstrated the first selective halogenation(s) of its π -conjugated core [24,25]. Beyond the preparation of original π -extended/conjugated BTI-based architectures, this

new class of compounds was also successfully used as the active component in the above-mentioned devices, thus highlighting, for the first time, their promising potential of **BTI** in organic electronics [24,26–28].

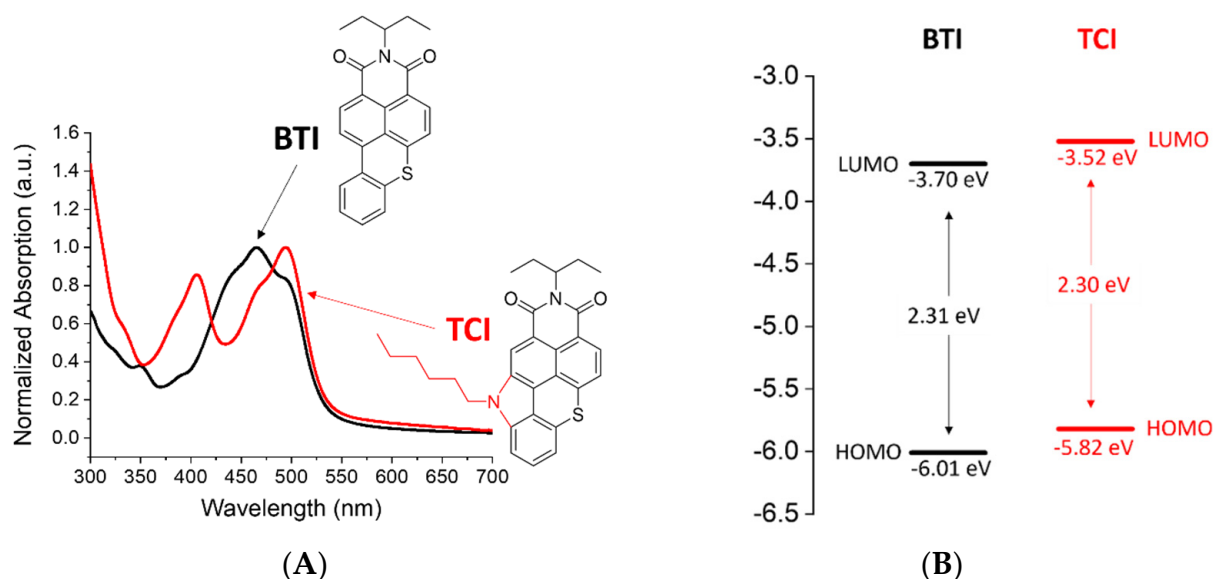


Figure 1. (A) Structures and solid state UV-visible spectra of **BTI** and **TCI**. (B) Frontier orbital energy diagram of both dyes in solid.

As a step forward in the chemical exploration of this dye, we lately achieved the *N*-annulation of its bay position, affording the thiochromenocarbazole imide, acronymed **TCI** (Figure 1A) [29]. Interestingly, incorporation of this fused, nitrogen-based 5-membered ring was found to induce a concomitant destabilization of both the highest occupied molecular orbital (HOMO) and the lowest unoccupied orbital (LUMO), resulting in an almost similar band gap (2.31 eV vs. 2.30 eV, Figure 1B).

In this study, thiophene-diketopyrrolopyrrole was selected as a π -bridge for its (i) ease of synthesis [30], (ii) compatibility with direct (hetero)arylation cross coupling reactions [31,32] and (iii) absorption in the visible that would, we hoped, shift those of the target compounds into the far red or near-infrared regions; an electromagnetic range of interest in many optoelectronic and bio-related applications (Figure 2) [33–36]. For instance, this *rylene imide-DPP-rylene imide* scaffold has been used successfully to develop non-fullerene acceptors for organic solar cells [37–39].

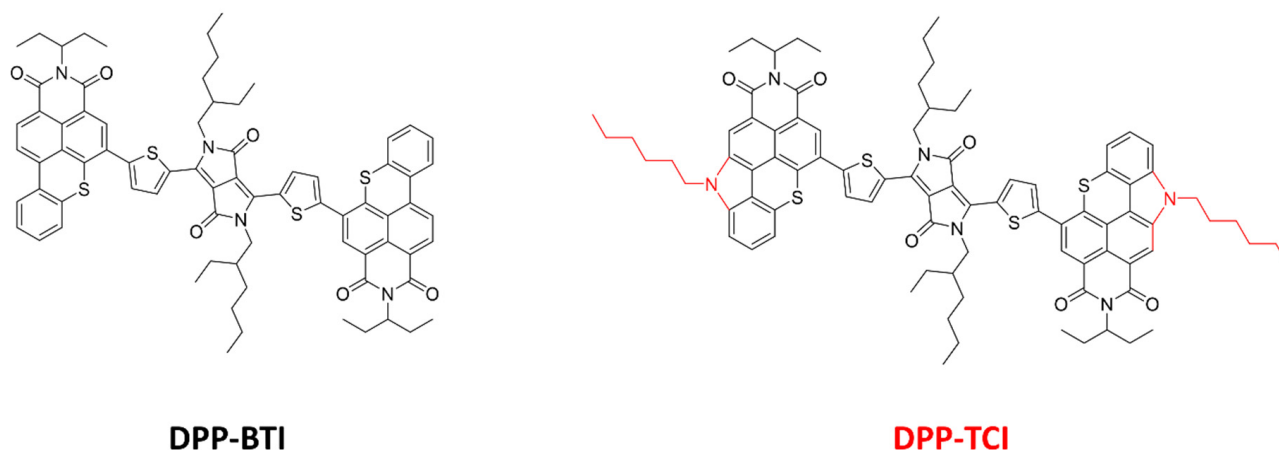
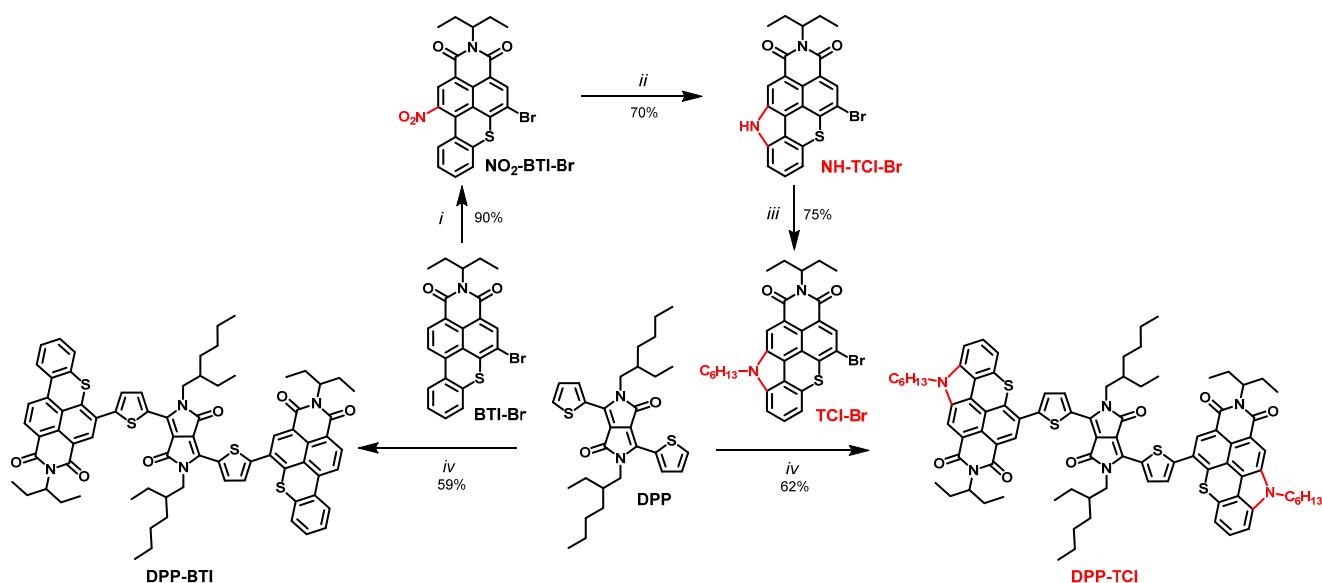


Figure 2. Structure of the two DPP based compounds studies in this contribution, namely **DPP-BTI** and **DPP-TCI**.

2. Results and Discussion

The synthetic route to the target compounds, namely **DPP-BTI** and **DPP-TCI**, is depicted in Scheme 1.



Scheme 1. Synthetic routes to **DPP-BTI** and **DPP-TCI**. (i) HNO₃, CH₂Cl₂, r.t. (ii) triphenylphosphine, DMF, reflux. (iii) K₂CO₃, 1-bromohexane, DMF, 120 °C. (iv) SiliaCat® DPP-Pd, K₂CO₃, PivOH, DMAc, 80 °C.

The materials were prepared following our previously reported procedure [24]; **BTI-Br** was selectively nitrated in its bay position prior to undergoing a Cadogan reductive cyclization reaction in presence of triphenylphosphine [29]. The resulting **NH-TCI-Br** was subsequently treated with 1-bromohexane under basic conditions to afford a *N*-alkylated and -annulated version of the **BTI-Br**, namely the **TCI-Br**. Both compounds were finally engaged in a heterogeneous palladium-catalyzed direct C-H arylation reaction with the **DPP** dye. Upon completion, both compounds were isolated from the crude by simple column chromatography on silica gel.

The molecules were found to be highly soluble in common organic solvents; their optical properties were first investigated in solution with comparison to their individual constituting building blocks, namely the **BTI**, **TCI** and **DPP** (Figure 3).

Interestingly, their characteristic absorption bands can be specifically attributed to the spectral features of their constituent π -extended molecules (**DPP-BTI** and **DPP-TCI**), even if shifted, to a greater or lesser extent, toward the longer wavelengths. Correlated to an improved donating effect, induced by the carbazole moiety, this redshift was indeed found to be more pronounced in the case of the **TCI**-based compound (**DPP-TCI**). Regarding the optical signatures of the rylene, a 13 nm shift was indeed observed for both characteristic bands of the *N*-annulated **TCI** (ca. 400 and 470 centered bands) when coupled to the **DPP** central core while only ca. 3 nm were measured for its **BTI** counterpart. Furthermore, the most drastic difference was observed for the band at lower energies, attributed to the **DPP** core, with a 41 nm shift for the **DPP-TCI** molecule (λ_{max} from 548 nm to 589 nm) vs. ca. 28 nm for the **DPP-BTI** molecule (λ_{max} from 548 nm to 576 nm). As a result, with an onset at ca. 640 nm, **DPP-TCI** exhibits a reduced band gap of ca. 0.06 eV compared to its **BTI**-based parent compound (λ_{onset} = 664 nm). On the other hand both molecule shows fluorescent properties in the far red-region (Table 1, Figure S10). With similar quantum yields (of ca. 60%), emission band of **DPP-TCI** also appears slightly redshifted (of ca. 6 nm) compared to that of **DPP-BTI**.

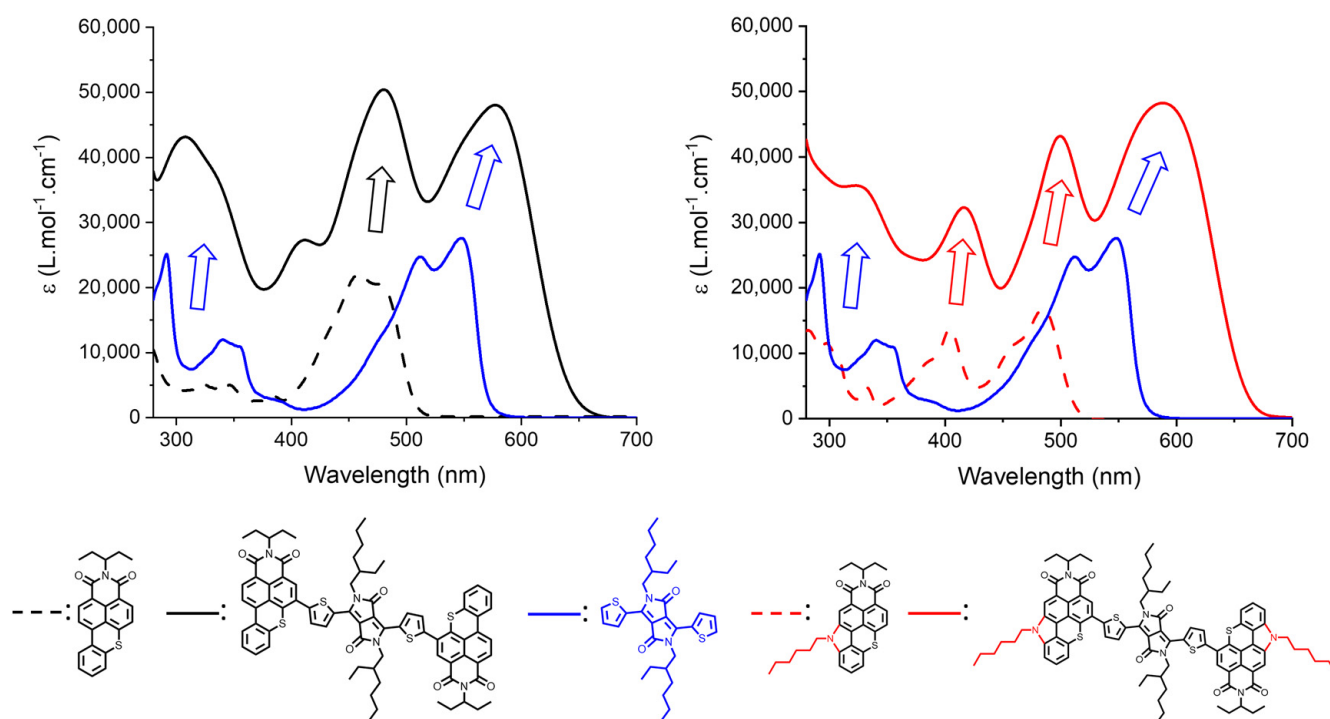


Figure 3. Comparison of the UV-visible spectra of **DPP-BTI** (black, full line) and **DPP-TCI** (red, full line) with their respective building blocks, i.e., the **BTI** (black, dash line), the **TCI** (red dash line) and the **DPP** (blue, full line) in CHCl_3 solution.

Table 1. Summary and comparison of the optical data of **DPP-BTI** and **DPP-TCI**.

Compound	λ_{max} Solution (nm)	ϵ ($\text{L}\cdot\text{mol}^{-1}\cdot\text{cm}^{-1}$)	λ_{em} Solution (nm)	Q_f^a	λ_{max} Film (nm)	Onset Film (nm)	E_g^{opt} Film (eV)	HOMO (eV) ^b	LUMO (eV) ^c
DPP-BTI	577	48,000	655	0.62	601	708	1.75	−5.68	−3.93
	480	50,000			488				
	411	27,000			426				
	308	43,000			337				
DPP-TCI	588	48,000	661	0.60	616	733	1.69	−5.45	−3.76
	499	43,000			505				
	416	32,000			425				
	324	35,500			340				

^a Measured using Coumarin-153 as reference ($\Phi_f = 0.45$ in MeOH); ^b Determined by photoemission spectroscopy in air (PESA); ^c LUMO = (HOMO) − E_g^{opt} (film).

In the thin film state, absorption spectra broaden and redshift (due to solid state aggregation), thus leading to even more reduced band gaps while maintaining the same trends observed in solution (Figure 4a and Table 1).

The greater impact on the HOMO level can be attributed to the improved donor character of the **TCI** blocks induced by the alkylated nitrogen atom constituting the carbazole ring while a reduced gap can be attributed to better conjugation along the backbone. The shallower HOMO level of **DPP-TCI** was also highlighted by the photovoltaic parameters observed in organic solar cells prepared from both the **DPP** based compounds, used as molecular donors. To do so, direct solar cells of architecture: ITO/PEDOT:PSS/active layer/LiF/Al were fabricated and tested under AM 1.5 G conditions. Once blended with (6,6)-Phenyl C_{71} butyric acid methyl ester (PC_{71}BM) best power conversion efficiencies were achieved in an optimal 1 to 3 weight to weight donor: acceptor ratio. As depicted in the respective current-to-tension (J-V) curves, plotted in Figure 5, higher open circuit voltage (V_{oc}) values and therefore efficiencies were systematically achieved with the **DPP-BTI** than **DPP-TCI**. (Table 2).

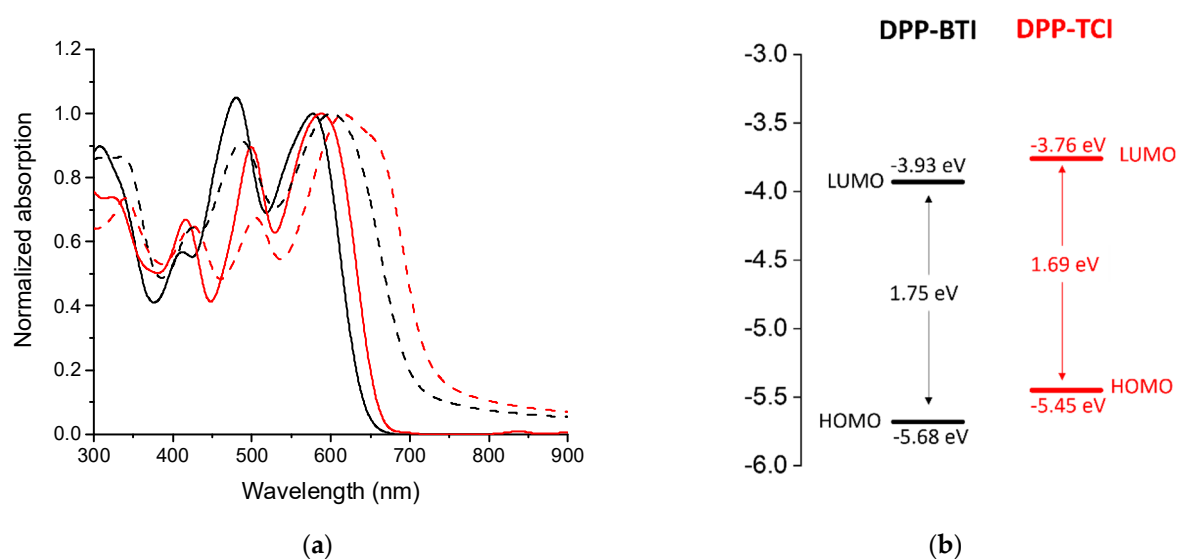


Figure 4. (a) Comparison of absorption spectra in solution (full line) and solid state (dash line) of **DPP-BTI** (black) and **DPP-TCI** (red). (b) Frontier orbital energy levels were estimated and compared, as shown in (b). The N-annulation of the **BTI** results in a concomitant destabilization (upward shift in energy) of both the HOMO ($\Delta_{\text{HOMO}} = 0.23$ eV) and LUMO ($\Delta_{\text{LUMO}} = 0.17$ eV) of the π -conjugated **DPP-TCI**, along with a reduction of the band gap ($\Delta E_g = 0.06$ eV).

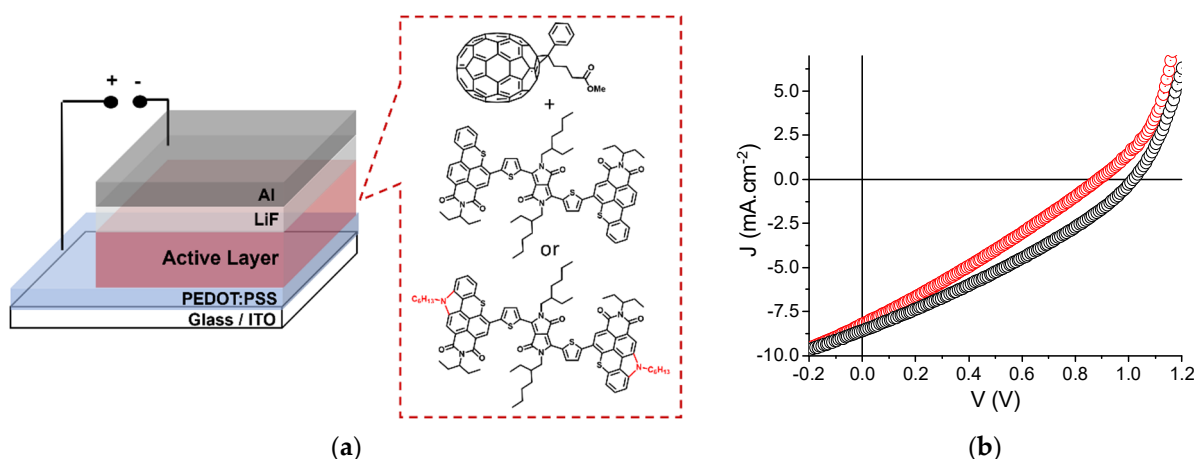


Figure 5. (a) Architecture of the organic solar cells used to evaluate the photovoltaic properties of **DPP-BTI** and **DPP-TCI**. (b) J-V curves of the best devices prepared either with **DPP-BTI** (black) and **DPP-TCI** (red) once blended with **PC₇₁BM** (in a 1:3 w:w donor:acceptor ratio).

Table 2. Best photovoltaic parameters (average values from 6 devices in brackets).

Compound	V _{oc} (V)	J _{sc} (mA·cm ⁻²)	FF (%)	PCE (%)
DPP-BTI	1.02 (1.01 ± 0.02)	8.55 (8.49 ± 0.07)	31 (29 ± 2)	2.70 (2.48 ± 0.18)
DPP-TCI	0.88 (0.87 ± 0.01)	8.19 (8.15 ± 0.08)	28 (27 ± 1)	2.01 (1.93 ± 0.07)

It is indeed usually generally accepted that the latter parameter (V_{oc}) is proportional to the difference between the LUMO of the acceptor (fullerene) and the HOMO of the donor (rylene imide **DPP** based compound), consistent with the observed trend in energy levels [40].

In order to understand the electronic structure of the molecules, density functional theory (DFT) calculations were performed. Optimized geometries are shown in Figure 6a, while the torsion angle between DPP and BTI or TCI units (measured as the dihedral angle in the bonds between atoms 1, 2, 3 and 4, highlighted in green in Figure 6a) was calculated and revealed a larger torsion angle for DPP-BTI (61.85°) than for DPP-TCI (50.14°), as depicted in Figure 6b. DFT results show that adding the N-annulated 5-membered ring in DPP-TCI increases (i) the energy of both the HOMO and LUMO orbitals of the molecule relative to DPP-BTI, consistent with HOMO and LUMO energy levels determined experimentally by PESA and UV-vis, and (ii) the HOMO energy to a greater extent than the LUMO, resulting in the reduction of the band gap.

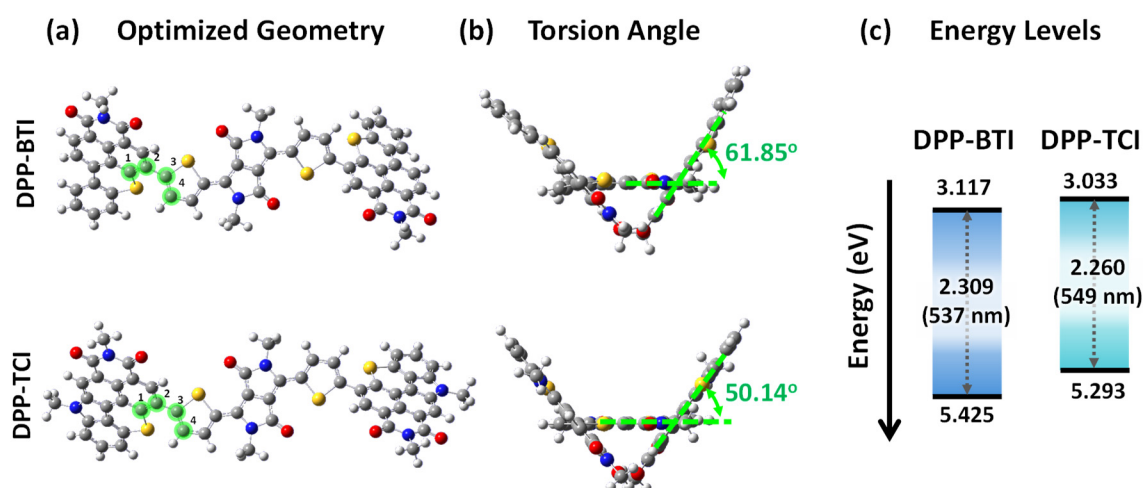


Figure 6. Optimized geometries of both DPP-BTI and DPP-TCI computed using the B3LYP density-functional treatment in the standard 6-311G basis set and values of the torsion angles measured between the rylene and the thiophene connector.

This decreased band gap in DPP-TCI (2.260 eV) compared to 2.309 eV for DPP-BTI, corresponds to HOMO—LUMO transitions occurring at 537 nm or 549 nm for DPP-BTI or DPP-TCI, respectively (Figure 6c). These calculated values are somewhat blueshifted compared to the measured values in solution (577 and 588 nm, respectively) however, gas-phase DFT calculations are expected to be blue-shifted compared to condensed phases (solution or film) and the difference in absorption onset and optical band gap between the two chromophores is in excellent agreement with the experimentally observed value (12 nm calculated red-shift vs. 11 nm observed red-shift).

These differences can be attributed to the relatively stronger electron-donating character of the annulated N-atom compared to the two C-H bonds that it replaces in DPP-BTI. N-alkyl groups are indeed known to be strongly electron-donating, additionally, the N-containing 5 membered ring incorporates N as a subunit of larger pyrrole, indole or carbazole structures, all of which are known as relatively electron-rich/electron-donating sub-structures. The measured frontier orbital energies and decrease in bandgap confirm the electron-donating character of the appended N-annular ring.

On the other hand, the decrease in torsion angle between the DPP and TCI groups can be rationalized as being caused by an increase in bond order between DPP and TCI relative to DPP and BTI; in other words, more double-bond character, better p-orbital overlap, and increased π -conjugation exists in the DPP-TCI bond, which manifests as a smaller torsion angle. It has been shown by Marder et al., in push-pull type chromophores, the bond length alternation (BLA) is decreased when stronger electron donating or electron withdrawing groups are used, leading to improved quinoid contribution to the ground state and corresponding increase in bond order between coupled aromatic rings [41,42]. Both DPP-BTI and DPP-TCI can be considered push-pull chromophores, DPP being a relatively electron-withdrawing moiety, while TCI shows a stronger electron-donating

character compared to **BTI**. Hence, the increased electron-donating character of **TCI** results in more double bond character between **DPP** and **TCI** than between **DPP** and **BTI**, despite identical steric interactions near the bond linking the two groups. This interpretation is consistent with the observed shortening of the bond length in **DPP-TCI** (1.468 Å) compared to **DPP-BTI** (1.473 Å), as seen in the computed optimized geometries.

3. Conclusions

As part of our endeavor to fully explore the potential of **BTI**-based derivatives, we have thus investigated the impact of *N*-annulation on the properties of π -extended structures, since similar band gaps were observed for both rylene parent structures (**BTI** and its *N*-annulated version, **TCI**). Thus, two π -conjugated compounds, based on a common thiophene-diketopyrrolopyrrole central core and end-capped with each rylene imide, were prepared by direct arylation. We observed that incorporation of the nitrogen-containing 5-membered ring in the **TCI** structure resulted in increased donor character and improved electronic conjugation along the backbone, resulting in shallower frontier orbital energy levels and a concomitant reduction of the band gap (approaching the near-infrared region in this case). The reduced band gap and increased π -conjugation in the **DPP-TCI** structure were attributed to a decrease in bond length alternation and an increase in the order of the bond linking **DPP** to **TCI** relative to the **DPP-BTI** bond. Hence, we show that a simple Cadogan cyclization turns out to be an easy and accessible strategy to fine-tune the energetics of **BTI**-based extended molecules, while at the same time providing additional orthogonal reactive sites at the carbazole N-atom available for functionalization with a variety of lateral side chains/groups. This work opens the door for further customization of **BTI**-based molecules, which can be conveniently optimized as absorbers, emitters and transport materials for a variety of optical and optoelectronic applications.

Supplementary Materials: The following supporting information, including synthetic procedures [24,29,43], spectroscopic data, photovoltaic fabrication details and computational data [44–46], can be downloaded at: <https://www.mdpi.com/article/10.3390/colorants2010002/s1>.

Author Contributions: Organic synthesis: T.G., J.M.A.C., P.J., J.B. and Y.Z. Characterization and device fabrication: S.A. and G.C.W., computational chemistry: B.W., supervision of S.A., S.T., P.B., ideas and writing: P.J., B.W. and C.C. All authors have read and agreed to the published version of the manuscript.

Funding: This research was funded by ANR-20-CE05-0029 (BTXI-APOGEE), Marie Skłodowska Curie Grant No.722651 (SEPOMO), ANR-18-EURE-0012 (EUR LUMOMAT, project AZA-BTX) and IRP CNRS MAPLE.

Institutional Review Board Statement: Not applicable.

Informed Consent Statement: Not applicable.

Data Availability Statement: Not applicable.

Acknowledgments: The ANR is acknowledged for the BTXI-APOGEE grant (ANR-20-CE05-0029). J.M.A.C. thanks the European Union's Horizon 2020 research and innovation program under Marie Skłodowska Curie Grant agreement No.722651 (SEPOMO). S.A. thanks the University of Tunis for her PhD grant. This research received no external funding. This work also received financial support under the EUR LUMOMAT project and the Investments for the Future program ANR-18-EURE-0012 (P.J.). C.C. and G.C.W. are also grateful to the CNRS for financial support provided through the IRP MAPLE.

Conflicts of Interest: The authors declare no conflict of interest.

References

1. Zhan, X.; Facchetti, A.; Barlow, S.; Marks, T.J.; Ratner, M.A.; Wasielewski, M.R.; Marder, S.R. Rylene and Related Diimides for Organic Electronics. *Adv. Mater.* **2011**, *23*, 268–284. [[CrossRef](#)] [[PubMed](#)]
2. Feng, J.; Jiang, W.; Wang, Z. Synthesis and Application of Rylene Imide Dyes as Organic Semiconducting Materials. *Chem.—A Eur. J.* **2018**, *13*, 20–30. [[CrossRef](#)] [[PubMed](#)]

3. Guo, X.; Facchetti, A.; Marks, T.J. Imide- and Amide-Functionalized Polymer Semiconductors. *Chem. Rev.* **2014**, *114*, 8943–9021. [[CrossRef](#)] [[PubMed](#)]
4. Al Kobaisi, M.; Bhosale, S.V.; Latham, K.; Raynor, A.M.; Bhosale, S.V. Functional Naphthalene Diimides: Synthesis, Properties, and Applications. *Chem. Rev.* **2016**, *116*, 11685–11796. [[CrossRef](#)] [[PubMed](#)]
5. Bhosale, S.V.; Al Kobaisi, M.; Jadhav, R.W.; Morajkar, P.P.; Jones, L.A.; George, S. Naphthalene diimides: Perspectives and promise. *Chem. Soc. Rev.* **2021**, *50*, 9845–9998. [[CrossRef](#)] [[PubMed](#)]
6. Takenaka, S. Application of naphthalene diimide in biotechnology. *Polym. J.* **2021**, *53*, 415–427. [[CrossRef](#)]
7. Zhou, Y.; Han, L. Recent advances in naphthalenediimide-based metal-organic frameworks: Structures and applications. *Coord. Chem. Rev.* **2021**, *430*, 213665. [[CrossRef](#)]
8. Cheng, P.; Zhao, X.; Zhan, X. Perylene Diimide-Based Oligomers and Polymers for Organic Optoelectronics. *Acc. Mater. Res.* **2022**, *3*, 309–318. [[CrossRef](#)]
9. Ali, S.; Gupta, A.; Shafiei, M.; Langford, S.J. Recent Advances in Perylene Diimide-Based Active Materials in Electrical Mode Gas Sensing. *Chemosensors* **2021**, *9*, 30. [[CrossRef](#)]
10. Kozma, E.; Catellani, M. Perylene diimides based materials for organic solar cells. *Dye. Pigment.* **2013**, *98*, 160–179. [[CrossRef](#)]
11. Würthner, F.; Saha-Möller, C.R.; Fimmel, B.; Ogi, S.; Leowanawat, P.; Schmidt, D. Perylene Bisimide Dye Assemblies as Archetype Functional Supramolecular Materials. *Chem. Rev.* **2016**, *116*, 962–1052. [[CrossRef](#)] [[PubMed](#)]
12. Chen, L.; Li, C.; Müllen, K. Beyond perylene diimides: Synthesis, assembly and function of higher rylene chromophores. *J. Mater. Chem. C* **2014**, *2*, 1938–1956. [[CrossRef](#)]
13. Schaack, C.; Evans, A.M.; Ng, F.; Steigerwald, M.L.; Nuckolls, C. High-Performance Organic Electronic Materials by Contorting Perylene Diimides. *J. Am. Chem. Soc.* **2022**, *144*, 42–51. [[CrossRef](#)] [[PubMed](#)]
14. Kuznetsova, L.I.; Piryazev, A.A.; Anokhin, D.V.; Mumyatov, A.V.; Susarova, D.K.; Ivanov, D.A.; Troshin, P.A. Disubstituted perylene diimides in organic field-effect transistors: Effect of the alkyl side chains and thermal annealing on the device performance. *Org. Electron.* **2018**, *58*, 257–262. [[CrossRef](#)]
15. Dayneko, S.V.; Cieplechowicz, E.; Bhojgude, S.S.; Van Humbeck, J.F.; Pahlevani, M.; Welch, G.C. Improved performance of solution processed OLEDs using N-annulated perylene diimide emitters with bulky side-chains. *Mater. Adv.* **2021**, *2*, 933–936. [[CrossRef](#)]
16. Hu, Y.; Gao, X.; Di, C.-A.; Yang, X.; Zhang, F.; Liu, Y.; Li, H.; Zhu, D. Core-Expanded Naphthalene Diimides Fused with Sulfur Heterocycles and End-Capped with Electron-Withdrawing Groups for Air-Stable Solution-Processed n-Channel Organic Thin Film Transistors. *Chem. Mater.* **2011**, *23*, 1204–1215. [[CrossRef](#)]
17. Takimiya, K.; Nakano, M. Thiophene-Fused Naphthalene Diimides: New Building Blocks for Electron Deficient π -Functional Materials. *Bull. Chem. Soc. Jpn.* **2018**, *91*, 121–140. [[CrossRef](#)]
18. Jones, B.A.; Facchetti, A.; Wasielewski, M.R.; Marks, T.J. Effects of Arylene Diimide Thin Film Growth Conditions on n-Channel OFET Performance. *Adv. Funct. Mater.* **2008**, *18*, 1329–1339. [[CrossRef](#)]
19. Grayshan, P.H.; Kadhim, A.M.; Peters, A.T. Heterocyclic derivatives of naphthalene-1,8-dicarboxylic anhydride. Part III. Benzo[k,l]thioxanthene-3,4-dicarboximides. *J. Heterocycl. Chem.* **1974**, *11*, 33–38. [[CrossRef](#)]
20. Kadhim, A.M.; Peters, A.T. A new intramolecular cyclisation reaction—I: Novel synthesis of benzo(k,l)thioxanthene-3,4-dicarboxylic anhydride and derived dyestuffs. *Tetrahedron* **1974**, *30*, 2245–2249. [[CrossRef](#)]
21. Tong, J.-D.; Moffitt, M.; Huang, X.; Winnik, M.A.; Rytz, R.A. Use of a dye-labeled ethylene-butene copolymer as a tracer in laser scanning confocal fluorescence microscopy studies of thermoplastic olefins. *J. Polym. Sci. Part A Polym. Chem.* **2001**, *39*, 239–252. [[CrossRef](#)]
22. Kadhim, A.M.; Mak, K.H.; Peters, A.T. New Dyes and Intermediates for Synthetic-polymer Fibres. 7,7-Dioxo-Benzo(K, /)thioxanthene-3,4-dicarboxylic Acid Imides. *J. Soc. Dye. Colour.* **1982**, *98*, 56–58. [[CrossRef](#)]
23. Mao, P.; Qian, X.; Zhang, H.; Yao, W. Benzothioxanthene dyes as fluorescent label for DNA hybridization: Synthesis and application. *Dye. Pigment.* **2004**, *60*, 9–16. [[CrossRef](#)]
24. Josse, P.; Li, S.; Dayneko, S.; Joly, D.; Labrunie, A.; Dabos-Seignon, S.; Allain, M.; Siegler, B.; Demadrille, R.; Welch, G.C.; et al. Bromination of the benzothioxanthene Bloc: Toward new [small pi]-conjugated systems for organic electronic applications. *J. Mater. Chem. C* **2018**, *6*, 761–766. [[CrossRef](#)]
25. Dalinot, C.; Simón Marqués, P.; Andrés Castán, J.M.; Josse, P.; Allain, M.; Abad Galán, L.; Monnereau, C.; Maury, O.; Blanchard, P.; Cabanetos, C. Regioselective Monohalogenation and Homo/Hetero Dihalogenation of Benzothioxanthene Monoimide. *Eur. J. Org. Chem.* **2020**, *2020*, 2140–2145. [[CrossRef](#)]
26. Payne, A.-J.; Rice, N.A.; McAfee, S.M.; Li, S.; Josse, P.; Cabanetos, C.; Risko, C.; Lessard, B.H.; Welch, G.C. Donor or Acceptor? How Selection of the Rylene Imide End Cap Impacts the Polarity of π -Conjugated Molecules for Organic Electronics. *ACS Appl. Energy Mater.* **2018**, *1*, 4906–4916. [[CrossRef](#)]
27. Dayneko, S.V.; Hendsbee, A.D.; Cann, J.R.; Cabanetos, C.; Welch, G.C. Ternary organic solar cells: Using molecular donor or acceptor third components to increase open circuit voltage. *New J. Chem.* **2019**, *43*, 10442–10448. [[CrossRef](#)]
28. Andrés Castán, J.M.; Dalinot, C.; Dayneko, S.; Abad Galán, L.; Simón Marqués, P.; Alévêque, O.; Allain, M.; Maury, O.; Favereau, L.; Blanchard, P.; et al. Synthesis, characterization and use of benzothioxanthene imide based dimers. *Chem. Commun.* **2020**, *56*, 10131–10134. [[CrossRef](#)]

29. Castán, J.M.A.; Amruth, C.; Josse, P.; Galan, L.A.; Marqués, P.S.; Allain, M.; Maury, O.; Le Bahers, T.; Blanchard, P.; Monnereau, C.; et al. Thiochromenocarbazole imide: A new organic dye with first utility in large area flexible electroluminescent devices. *Mater. Chem. Front.* **2022**, *6*, 1912–1919. [[CrossRef](#)]
30. Grzybowski, M.; Gryko, D.T. Diketopyrrolopyrroles: Synthesis, Reactivity, and Optical Properties. *Adv. Opt. Mater.* **2015**, *3*, 280–320. [[CrossRef](#)]
31. Josse, P.; Dayneko, S.; Zhang, Y.; Dabos-Seignon, S.; Zhang, S.; Blanchard, P.; Welch, G.C.; Cabanetos, C. Direct (Hetero)Arylation Polymerization of a Spirobifluorene and a Dithienyl-Diketopyrrolopyrrole Derivative: New Donor Polymers for Organic Solar Cells. *Molecules* **2018**, *23*, 962. [[CrossRef](#)] [[PubMed](#)]
32. Josse, P.; Chávez, P.; Dindault, C.; Dalinot, C.; McAfee, S.M.; Dabos-Seignon, S.; Tondelier, D.; Welch, G.; Blanchard, P.; Leclerc, N.; et al. Thiophene vs thiazole: Effect of the π -connector on the properties of phthalimide end-capped diketopyrrolopyrrole based molecular acceptors for organic photovoltaics. *Dye. Pigment.* **2017**, *137*, 576–583. [[CrossRef](#)]
33. Li, Q.; Guo, Y.; Liu, Y. Exploration of Near-Infrared Organic Photodetectors. *Chem. Mater.* **2019**, *31*, 6359–6379. [[CrossRef](#)]
34. Beć, K.B.; Grabska, J.; Huck, C.W. Near-Infrared Spectroscopy in Bio-Applications. *Molecules* **2020**, *25*, 2948. [[CrossRef](#)]
35. Zhang, N.N.; Lu, C.Y.; Chen, M.J.; Xu, X.L.; Shu, G.F.; Du, Y.Z.; Ji, J.S. Recent advances in near-infrared II imaging technology for biological detection. *J. Nanobiotechnol.* **2021**, *19*, 132. [[CrossRef](#)]
36. Kaur, M.; Choi, D.H. Diketopyrrolopyrrole: Brilliant red pigment dye-based fluorescent probes and their applications. *Chem. Soc. Rev.* **2015**, *44*, 58–77. [[CrossRef](#)]
37. McAfee, S.M.; Payne, A.-J.; Hendsbee, A.D.; Xu, S.; Zou, Y.; Welch, G.C. Toward a Universally Compatible Non-Fullerene Acceptor: Multi-Gram Synthesis, Solvent Vapor Annealing Optimization, and BDT-Based Polymer Screening. *Sol. RRL* **2018**, *2*, 1800143. [[CrossRef](#)]
38. McAfee, S.M.; Dayneko, S.V.; Hendsbee, A.D.; Josse, P.; Blanchard, P.; Cabanetos, C.; Welch, G.C. Applying direct heteroarylation synthesis to evaluate organic dyes as the core component in PDI-based molecular materials for fullerene-free organic solar cells. *J. Mater. Chem. A* **2017**, *5*, 11623–11633. [[CrossRef](#)]
39. McAfee, S.M.; Dayneko, S.V.; Josse, P.; Blanchard, P.; Cabanetos, C.; Welch, G.C. Simply Complex: The Efficient Synthesis of an Intricate Molecular Acceptor for High-Performance Air-Processed and Air-Tested Fullerene-Free Organic Solar Cells. *Chem. Mater.* **2017**, *29*, 1309–1314. [[CrossRef](#)]
40. Widmer, J.; Tietze, M.; Leo, K.; Riede, M. Open-Circuit Voltage and Effective Gap of Organic Solar Cells. *Adv. Funct. Mater.* **2013**, *23*, 5814–5821. [[CrossRef](#)]
41. Marder, S.R.; Cheng, L.T.; Tiemann, B.G.; Friedli, A.C.; Blanchard-Desce, M.; Perry, J.W.; Skindhøj, J. Large first hyperpolarizabilities in push-pull polyenes by tuning of the bond length alternation and aromaticity. *Science* **1994**, *263*, 511–514. [[CrossRef](#)] [[PubMed](#)]
42. Marder, S.R.; Gorman, C.B.; Tiemann, B.G.; Perry, J.W.; Bourhill, G.; Mansour, K. Relation Between Bond-Length Alternation and Second Electronic Hyperpolarizability of Conjugated Organic Molecules. *Science* **1993**, *261*, 186–189. [[CrossRef](#)] [[PubMed](#)]
43. Woo, C.H.; Beaujuge, P.M.; Holcombe, T.W.; Lee, O.P.; Fréchet, J.M.J. Incorporation of furan into low band-gap polymers for efficient solar cells. *J. Am. Chem. Soc.* **2010**, *132*, 15547–15549. [[CrossRef](#)] [[PubMed](#)]
44. Frisch, M.J.; Trucks, G.W.; Schlegel, H.B.; Scuseria, G.E.; Robb, M.A.; Cheeseman, J.R.; Scalmani, G.; Barone, V.; Petersson, G.A.; Nakatsuji, H.; et al. *Gaussian 09, Revision A.02*; Gaussian, Inc.: Wallingford, CT, USA, 2016.
45. Becke, A.D. Density-Functional Thermochemistry. III. The Role of Exact Exchange. *J. Chem. Phys.* **1993**, *98*, 5648–5652. [[CrossRef](#)]
46. Stephens, P.J.; Devlin, F.J.; Chabalowski, C.F.; Frisch, M.J. Ab Initio Calculation of Vibrational Absorption and Circular Dichroism Spectra Using Density Functional Force Fields. *J. Phys. Chem.* **1994**, *98*, 11623–11627. [[CrossRef](#)]

Disclaimer/Publisher’s Note: The statements, opinions and data contained in all publications are solely those of the individual author(s) and contributor(s) and not of MDPI and/or the editor(s). MDPI and/or the editor(s) disclaim responsibility for any injury to people or property resulting from any ideas, methods, instructions or products referred to in the content.